Spontaneous locking of optical vortices in coupled semiconductor lasers

Yoav Yadin,[1] Jacob Scheuer,[2,*] Yoav Gross,[1] and Meir Orenstein[1]
[1]*Department of Electrical Engineering, Technion, Haifa 32000, Israel*
[2]*School of Electrical Engineering, Tel-Aviv University, Ramat Aviv 69978, Israel*
(Received 4 February 2013; published 2 September 2014)

Non-conventional emission of light, comprising engaged rotating light cogs, is measured and analyzed. The source of this unique emission is an array of coupled surface emitting lasers, each emitting an optical vortex. The complex rotating light structures are formed spontaneously by specific combinations of the individual vortices, each carrying two types of "charge": orbital angular momentum (± 1 topological charge) and a relative engagement phase (0 or π). These charges determine the specific form in which the individual rotating fields are engaged to generate the emanated light gear. The experimentally observed formations and dynamic evolution of the light gears stem from the complex nonlinear dynamics of the coupled rotating-field emitters, a mechanism which we have successfully modeled and utilized for interpreting the obtained results. The engaged light gears can be used in controlled generation and transmission of multiple degrees of freedom photons, for high-bit-rate classic and quantum telecommunications, particle manipulation, and super-resolution imaging.

DOI: 10.1103/PhysRevA.90.033803 PACS number(s): 42.50.Tx, 42.55.Px, 42.55.Sa, 42.60.Jf

I. INTRODUCTION

Generating photons, or the equivalent classical light cavity modes, with multiple and diverse degrees of freedom, is of both fundamental and practical importance. Accurate control over the fundamental properties of the spatial distribution (amplitude and phase) of single and multiple photons is beneficial for numerous applications such as multiple-bit quantum transmission and computing [1–7], high-bit-rate telecommunications [8,9], subwavelength fluorescence microscopy [10,11], multiple particles manipulation, and more [12–23]. The orbital angular momentum (OAM) of light constitutes such flexible and highly complex degree of freedom. In addition to the polarization (helicity) state of a photon, which is related to its spin and is a superposition of binary states (± 1 in angular momentum units), the OAM originating from the spatial distribution of the optical field can in principle carry any integer topological "charge" value [24–29]. It was shown, however, that singular OAM charge larger than 1 is unstable under propagation in nonlinear or turbulent media, resulting in its decomposition to a combination of charge 1 vortices [24,25] such that the multilevel OAM information is carried by an array of unit charges, spatially distributed over the optical beam. The formation of optical vortices in nonlinear media has also attracted much attention and a rich variety of OAM carrying beams such as vortex solitons [30–33], azimuthons [34,35], and rotating soliton necklaces [36–38] have been studied and demonstrated. Here, we measure experimentally and analyze non-conventional spontaneously formed, complex emission patterns of light consisting of engaged rotating light cogs ("gears"), where each of the latter is emanating from a single light-vortex laser source with a unit topological charge (a source having a phase singularity at its center of symmetry and the field rotating about the center with a unit angular momentum—hence the light gear). This is a unique scenario in which two distinct coupling mechanisms (relative phase locking and rotation locking) are acting simultaneously and generating rich and complex patterns. The resulting coupled vortex beams are emitted from an array of vertical cavity surface emitting lasers (VCSELs), which constitute an excellent microlaboratory for experimental studies of nonlinearly coupled oscillator networks. This is an experimental demonstration of spontaneous headedness symmetry breaking generated by the nonlinear dynamics of the coupled oscillators' network. The electromagnetic field of the engaged light gears carries multiple discrete "charges" of two types—OAM (optical vortices) of topological charge ± 1 and relative phases (0 or π). The OAM additional degree of freedom results in a unique coupling "algebra" which differs fundamentally from the coupling rules known for conventional coupled laser arrays [39] and opens up new avenues for richer and more complex interactions. An indication to the potential complexity of the outcome field pattern may be inferred from Ref. [40] which depicts field patterns resulting from noncoaxial combination (by means of a beam splitter) of two vortices generated artificially by holographic mask. However the scenario analyzed in [40] differs fundamentally than that discussed here, namely the interactions that generate spontaneously the gear patterns. The emphasis of our study is on the spontaneous formation of the complex vortex configuration and the *intricate nonlinear interaction*s between the vortices emitted from each VCSEL. Because of the nonlinear nature of the interaction, *diverse* vortex configurations could be emitted from a single device, simply by changing a control parameter, which in our case is the injected current. In addition, the nonlinear interaction facilitates multistability phenomena, in contrast to the linear scheme presented in [40] which dictates a unique relation between the holographic mask and the vortex configuration.

The field is thus generated by complex coupling dynamics of nonlinear optical oscillators according to the following scheme: An optical metallic antenna array located on the laser chip within the emission field of a laser (~ 2 μm away from the emitting layer; see Fig. 1), is reseeding the gain medium by backscattering the laser emission, according to the array pattern, thus initiating nonlinear dynamics and spontaneous symmetry breaking that generate the specific

*kobys@eng.tau.ac.il

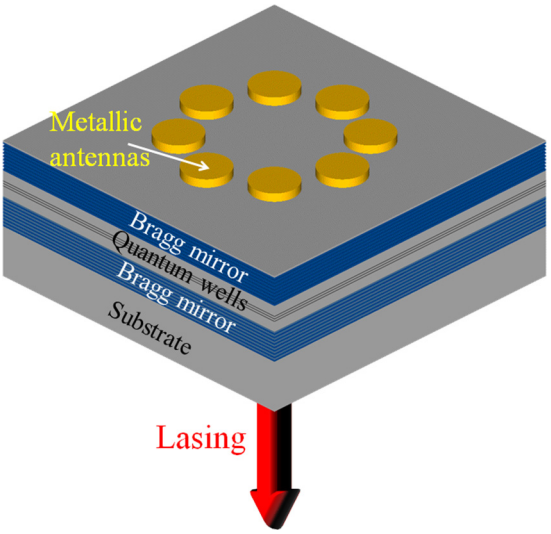

FIG. 1. (Color online) Schematic of the VCSEL arrays used for the observation of the locked light gears.

stable engaged light gears with preferred angular momenta and coupling phases. The theoretical analysis of this coupling phenomenon necessitates the introduction of expanded "base functions" which include the two counter-rotating vortex states (of unit angular momentum) in each laser element. This is a substantial modification of currently employed laser modal analysis, employing a "standing-waves" function basis which is less adequate for describing the vortex patterns. In our study, we find good agreement between measured and modeled light gears consisting of two, three, four, and five coherently locked vortices.

Coherent locking in laser arrays, in general, is a broad research field, which is both of fundamental scientific interest (e.g., [41]) and practical applications, primarily for high-power coherent sources [42,39]. Regular coupled semiconductor laser arrays (each laser is emitting the fundamental mode) exhibit predominantly antiphase supermodes (relative phase of neighboring elements fields is π). This tendency is unfortunate for the purpose of generating single-lobed far field, and substantial efforts were focused on attempts to coherently lock laser arrays in phase (all lasers have identical phases) [42–48].

Figure 1 illustrates the schematic of a vertical cavity surface emitting laser (VCSEL) array which was employed in our experiment. Both linear and cyclic arrays were studied in a scenario in which each VCSEL emits a single optical vortex. The basic element in our experiments is thus a single VCSEL emitting a single-charge "± 1" vortex. Spontaneous lasing of optical vortices has been demonstrated in large-area lasers, e.g., sodium vapor laser [49], solid-state lasers [50], and in VCSELs [51]. This latter complex emission was shown to stem from the intrinsic nonlinearity of the VCSELs that is locking preferred combinations of the eigenmodes of a parabolic index of refraction profile. However, as we are interested in generating light distributions with *controlled* "bit" patterns, we employ here a preconfigured array of relatively small-area VCSELs, each of the latter emitting a single optical vortex, while all of the vortices in the array are engaged by spontaneous mutual locking. In the resulting field pattern, each of the individual laser elements possesses two "bits" of information—the vortex charge (± 1 in units of angular momentum), and the relative phase charge in the constellation, (0 or 1 in units of π). The two types of charges are related to two different types of phase singularities of the optical field (point and line dislocation, respectively).

The rest of this paper is organized as follows. In Sec. II we describe the experimental setup and report on the experimentally observed light gears. In Sec. III we present the nonlinear dynamical model based on coupled rate equations and in Sec. IV we describe the engaged gear patterns predicted by the model. In Sec. V we study theoretically the stability properties of the obtained patterns and reconcile the differences between the experimental and theoretical results. In Sec. VI we discuss the results and summarize.

II. EXPERIMENTAL RESULTS

Experimental characterization of the light gears was performed by recording the transverse intensity patterns emerging from coherently locked arrays of proton implanted, medium-area VCSELs (10–20 $\mu\mu$ in diameter). The active layer of these VCSELs consisted of three 8-nm $In_{0.2}Ga_{0.8}As$ wells, emitting at $\sim$0.95 μm. The array structure was imposed by depositing an Au optical microantenna array on the back Bragg mirror of the VCSEL, where each antenna element is defining an effectively single laser. A complete description of the antenna patterns fabrication is given in Ref. [42]. This antenna array is excited by the emitted field from the laser structure and scatters its self-field pattern back to the laser gain medium, thus seeding the pattern for the subsequent emission. The emitted field patterns were examined at room temperature under pulsed, quasi-cw, electrical current injection [pulse width of 300–1000 ns with repetition rate of 200 kHz was selected to get best visibility of the pattern by a charge-coupled device (CCD) camera]. It should be emphasized that the locked vortices configurations were observed over a relatively wide range of injection currents and pulse widths (see figure captions for the specific values). This remarkable result is highly important both fundamentally, as it highlights the robustness of the observed patterns, and practically as it facilitates exploiting them for various applications. We characterized the lasing pattern (LP) (high-resolution imaging of the light intensity pattern at the gain layer), far field (FF), the spectrally resolved LP intensity distributions, and the interference pattern of the light gears with a reference beam to resolve their AOM structure [52].

Figure 2 depicts the LP of a vortex-scape emanated from linear and cyclic VCSEL arrays, where each element in these arrays is emitting predominantly a single optical vortex. Referring to the simplest case of a vortex dimer—where each vortex element carries two types of charges (AOM and relative phase)—there are four possible combinations. Below, we describe in detail the "algebra" of engaging two vortex sources (light gears) to generate a dimer. The calculated field distributions, LP, FF, and interference (with a skewed plane wave) intensity patterns of the possible combinations are depicted in Fig. 3.

The relative rotation of the in-phase coupled vortices in Fig. 3(a) exhibits the expected opposite headedness (as in

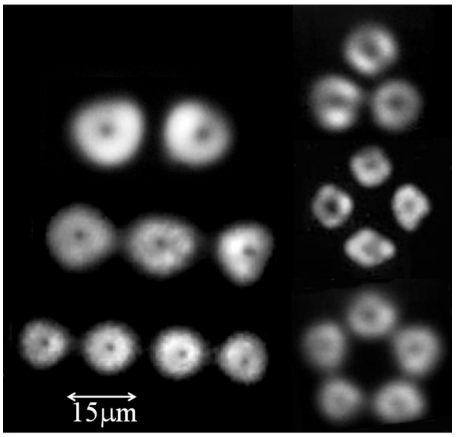

FIG. 2. Imaged intensity distributions of light gears made of coupled vortex patterns, as emitted from a variety of linear and cyclic VCSEL arrays. $I_p \approx 50$–200 mA, $\tau_{\text{pulse}} \approx 300$–$1000$ ns.

mechanical gears). However, the two (same phase) vortices depicted in Fig. 3(b) exhibit identical OAM charge sign. A closer examination of the interference pattern reveals an additional oppositely charged vortex, located between the main vortices, which serves as a "transmission wheel cog" allowing proper rotation transfer from one vortex to the other. In the two antiphase dimer configurations [Figs. 3(c) and 3(d)] the π phase discontinuity in between the vortices provides the phase adjustment necessary for satisfying field continuity.

Experimentally, we observed two of the four possible light gears (the spontaneous emergence of the specific configurations and their stability are discussed in Secs. IV and V): In-phase vortices with opposite vorticity [Fig. 4(b)], a pattern which is unique in the context of coupled lasers arrays because of its in-phase structure. For the dimers, we determined those

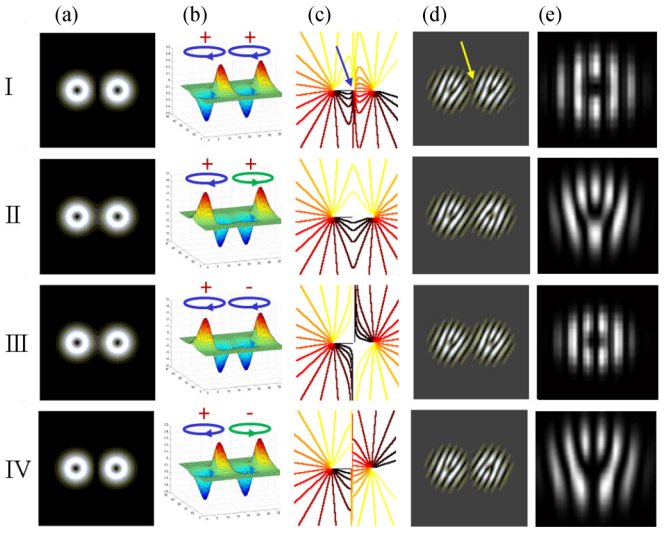

FIG. 3. (Color online) Calculated LP(a); field distribution (b); equiphase lines (bright yellow, 0, to dark red, 2π) (c); interferograms (d); FF (e) of the four possible engagement configurations of two vortices: (I) in-phase, identical vorticity; (II) antiphase, identical vorticity; (III) in-phase, opposite vorticity; (IV) antiphase, opposite vorticity. Arrows indicate additional vortex.

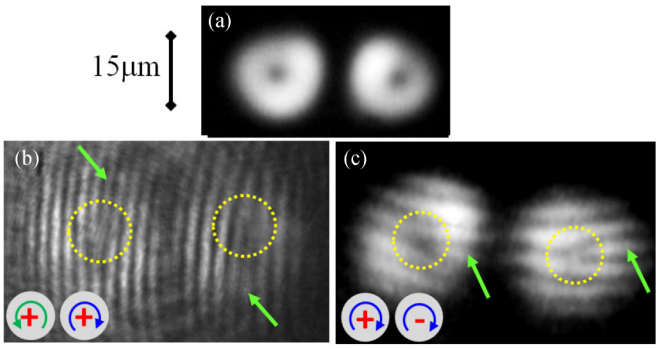

FIG. 4. (Color online) Measured LP (a) and near-field interferograms of two different pairs of coupled VCSELs. (b) Opposite charges in-phase gear, $I_p = 150$ mA, $\tau_{\text{pulse}} = 800$ ns; (c) identical charges antiphase gear $I_p = 100$ mA, $\tau_{\text{pulse}} = 1000$ ns. $I_{\text{th}} = 50$ mA.

bit patterns by measuring the interferograms of the emission with a tilted plane wave (Fig. 4), where the discontinuities in the intensity patterns associated with the singularities can be easily detected. Such measurements, however, become cumbersome for larger arrays. Fortunately, the FF is uniquely identifying the complete bit pattern of the field [e.g., Fig. 3(f)] and a specific example of measured FF for the pair of antiphase vortices with the same vorticity [corresponding to Fig. 4(c)] is shown in Fig. 5.

The main body of the experimental study was performed on cyclic VCSEL arrays, constituting an interesting platform, because of the phase restrictions imposed by the cyclic symmetry. We observed a clear difference between the emission patterns from even and odd laser arrays emitting vortices. Arrays consisting of an even number of lasers exhibited an antiphase gear pattern with identical OAM charges. Row II of Figures 6(c) and 6(d) depicts, respectively, the experimentally observed and the theoretically calculated FF pattern of four vortices. The good agreement between the theory and experiment is evident.

While the emission properties of cyclic arrays consisting of an even number of vortex sources are antiphase locked, as in a regular laser array (emitting the fundamental mode), the case of the odd cyclic array is different. Cyclic arrays comprising an odd number of regular (not vortex) lasers cannot display the antiphase emission because of phase frustration [53]. As a result, they exhibit symmetry breaking and the emitted pattern consists of an even number of lobes ($M \pm 1$, where M is the

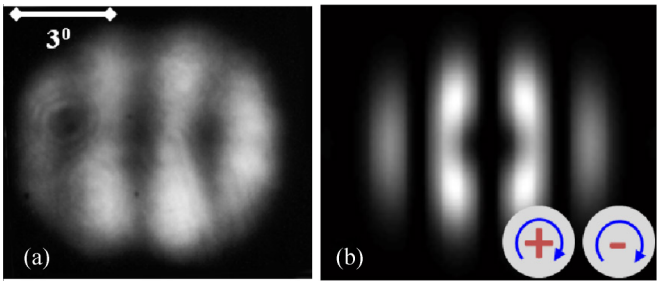

FIG. 5. (Color online) Measured (a) and calculated (b) FF intensity pattern of the antiphase identical vorticity dimer depicted in Fig. 4. $I_p = 100$ mA, $\tau_{\text{pulse}} = 1000$ ns.

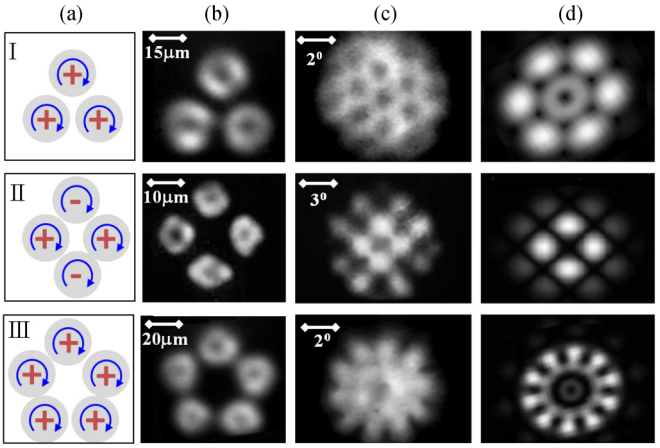

FIG. 6. (Color online) Schematics (a), measured LP (b) and FF intensity (c) patterns, and the calculated FF (d) intensity patterns of cyclic arrays. For the odd arrays (I, III) the calculated FF intensity pattern is of identical charges in-phase locked vortices and for the even (II) antiphase locked vortices with identical charges. Pump conditions: (I) $I_p = 50$ mA, $\tau_{\text{pulse}} = 1000$ ns; (II) $I_p = 150$ mA, $\tau_{\text{pulse}} = 800$ ns; (III) $I_p = 150$ mA, $\tau_{\text{pulse}} = 400$ ns.

number of lasers in the array) [53]. In the current experiment, the odd cyclic array of vortices exhibited an odd number of vortex beams [Figs. 6(a) and 6(c)], which were locked in phase, and with identical OAM charges. Figures 6(c) and 6(d) (rows I and III) compare the calculated and measured FF patterns for these cases, demonstrating a good match.

One of the unique characteristics of the in-phase vortices pattern is the formation of counter-rotating vortices between adjacent laser beams, thus providing the necessary transfer of the rotation of the fields as was explained for the dimer case. Due to the closed (circular) configuration, an additional vortex at the center of symmetry of the array must support this planetary gear. The equiphase contours of the field emanated from a five-elements cyclic array (calculated from the complete dynamical nonlinear model described below) are depicted in Fig. 7(a) with a cartoon of a mechanical equivalent for better visualization of the complex rotating fields [Fig. 7(b)].

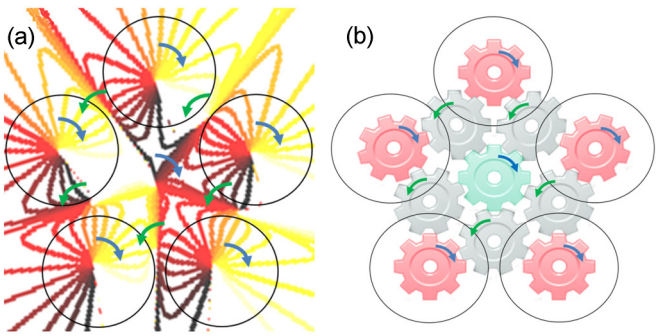

FIG. 7. (Color online) The highly complex gear, generated from coupling of five vortices (a) the equiphase lines as calculated from the model (from bright yellow to dark red); (b) an equivalent mechanical gear for illustration. Blue (green) arrows indicate clockwise (anticlockwise) rotation of the vortex (gear).

III. THEORETICAL MODEL

In order to comprehend the formation of these complex patterns and the stable evolution of only very few of the possible "bit patterns," we developed a theoretical model based on the rate equations for the electromagnetic field and carriers in a semiconductor emitter [53].

The model is more extensive than typical models analyzing the emission patterns from coupled emitters found in the literature. Most of the latter use the discrete approach—where the laser field in each emitter is fixed (usually the basic mode) and the dynamics is only of the discrete coefficients of the various lasers in the evolved field. In this approach, the coupling coefficients, the gain, and the fields are not spatially fixed but are dynamical variables. Furthermore a nearest-neighbor approximation is usually employed, which takes into account only the interaction of an emitter element with its nearest-neighboring elements which simplifies the calculations significantly. In our case, where multimode emission from each laser element is an essential ingredient, spatial hole burning and spatial mode competition over the gain are dominant effects and must be included. In addition no nearest-neighbor approximation is made.

The rate equations for the electric field and charge carriers' density in a semiconductor vertical cavity laser emitter are [53]

$$\dot{\mathrm{E}}(x,y) = \frac{c}{\mu}\left[\Gamma(1 - iR)\, g(x,y) - \alpha(x,y)\right]\mathrm{E}(x,y), \quad (1)$$

$$\dot{N}(x,y) = \frac{J(x,y)}{ed} - \frac{N(x,y)}{\tau} - \Gamma g(x,y)\frac{\mu\varepsilon_0}{2k_0}|\mathrm{E}(x,y)|^2, \quad (2)$$

$$g(x,y) = \frac{a\left[N(x,y) - N_{\text{tr}}\right]}{1 + \varepsilon'|\mathrm{E}(x,y)|^2}, \quad \varepsilon' = \varepsilon\frac{\varepsilon_0\mu^2}{2\hbar\omega}, \quad (3)$$

where $\mathrm{E}(x,y)$ is the transverse complex electric field distribution, c the speed of light, μ the refractive index, Γ the longitudinal confinement factor (the gain comprises only three 8-nm quantum wells out of the entire half-wavelength cavity), R the antiguiding factor, $g(x,y)$ the transverse gain distribution, and $\alpha(x,y)$ the transverse loss distribution, which includes internal losses but also the seeding nanoantennas spatial pattern. $N(x,y)$ is the charge carrier density distribution, e the electron charge, d the thickness of the active layer (the quantum wells), τ the electron lifetime, ε_0 is the vacuum permeability, k_0 the vacuum wave number, a the differential gain coefficient, N_{tr} the charge carrier density at lasing threshold, ε the photon number saturation coefficient, ω the lasing frequency, and $J(x,y)$ the injection current density profile at the quantum wells plane which is obtained as a steady-state solution of the following diffusion equation, starting from the initial circular injection current density:

$$\frac{dJ(x,y)}{dt} = D\nabla^2 J(x,y) + J_0(x,y) - \frac{J(x,y)}{\tau}, \quad (4)$$

where D is the diffusion coefficient and $J_0(x,y)$ the current source density (assumed to be circular). Another unique and crucial ingredient in our modeling is the assumption that the emitted pattern from each emitter element is a coherent superposition of the charge $+1$ and charge -1 vortex modes,

thus yielding a total of $2M$ base functions, where M is the number of the laser elements in the array. The total field profile emitted from the array is given by

$$\mathrm{E}(x,y) = \sum_{n=1}^{2M} E_n \psi_n(x,y), \tag{5}$$

where $\psi_n(x,y)$ is the transverse electrical field distribution of the nth mode, and E_n is the complex coefficient of that mode. This assumption is plausible for our scenario because the basic mode, which is lasing near threshold, burns a spatial hole in the gain at the center of each emitter element, thus enabling the stable operation of the two vortex (donut) modes that are using the circumferential gain, and are in charge of the complex patterns reported here.

Solving the equations yields a nonlinear eigenvalue problem for the steady-state mode coefficients:

$$A^{-1}B(E)\,E = i\Omega E, \tag{6}$$

where

$$A_{mn} = \iint \psi_m^* \psi_n dx dy, \tag{7}$$

$$B_{mn} = \frac{c}{\mu}\iint \psi_m^*[\Gamma(1-iR)g(x,y) - \alpha(x,y)]\psi_n dx dy, \tag{8}$$

$$E = (E_1, E_2, \ldots, E_{2M},)^T. \tag{9}$$

Assuming that each laser emits a superposition of a charge $+1$ and -1 vortex (primarily no symmetry breaking between the two headedness) and denoting the electric field of the charge $+1$ (-1) vortex within the mth VCSEL by V_{m+}, (V_{m-}), the overall emitted electric field can be written as

$$E = \sum_{m=1}^{M}(C_{m+}V_{m+} + C_{m-}V_{m-}), \tag{10}$$

where the field coefficients C_{m+} and C_{m-} must be determined.

Substituting the electric field into the rate equations yields a set of temporal evolution equations for the coefficients:

$$\frac{\partial}{\partial t}C_{n\pm}(t) = -\frac{c}{\mu}\alpha_{\mathrm{tot}}C_{n\pm} + \frac{c}{\mu}(1-iR)\Gamma \times \sum_{m=1,\,j=+,-}^{N} C_{mj}\iint g V_{mj} V_{\pm} da, \tag{11}$$

where α_{tot} is the loss and g the optical gain. Note that in obtaining (11) we have assumed that the carrier dynamics [Eq. (2)] can be adiabatically eliminated; otherwise the computational complexity is overwhelming. Essentially this means that changes in the field profile are assumed to be followed *immediately* by the gain. This assumption allows multiple formal steady-state solutions of Eqs. (1)–(4); however, as it does not reflect correctly the *dynamics* of the pattern formation, it does not show which of the formal solutions are stable, that is, experimentally observable. This issue is further discussed in Sec. V.

IV. RESULTS OF THE THEORETICAL MODEL

The set of nonlinear differential equations (11) were solved numerically and their steady-state solutions were obtained for a span of injection current levels. In order to excite and observe the various steady-state patterns, the equations were seeded with several initial conditions (initial values of the mode coefficients).

The model was applied to emitter arrays of two to five laser elements, each 10 μm in diameter, with 2 μm spacing (corresponding to the dimensions of the experimentally studied devices). The modes included the charge $+1$ and charge -1 vortex in each element, with a mode radius of 3.5 μm, again corresponding to the experimentally measured one.

Several steady-state configurations were found by applying the model machinery including all the experimentally observed engaged gear patterns, but also additional configurations which were not observed. A comprehensive analysis of the results shows that all the theoretically predicted emission patterns comply with a set of simple guidelines explaining the selection rules for locking configuration at different injection current levels. These guidelines are outlined at the end of this section, following a detailed description of the theoretical results for each class of arrays.

In the following, we elaborate on the theoretical results for two cases—the dimer emitter and the cyclic five-elements emitter. We then use these results to derive and exemplify the engagement rules of the light gears.

A. The dimer based light gears

The steady-state supermodes predicted by the model as a function of the injection current, normalized to the threshold current, are summarized in Table I. All four possible configurations of two vortices can be obtained theoretically [two of them, (b) and (c), were observed experimentally], in addition to the double TEM_{10} mode.

For low injection currents (1–$1.2I_{\mathrm{th}}$), the steady-state pattern consists of a double-lobe emission from each laser [configuration (a) in Table I]. At higher injection currents (1.5–$2.5I_{\mathrm{th}}$) the identical charge in-phase and opposite charge antiphase supermodes evolve. These are the configurations in which the field exhibits zero in the interelement spacing. At $I = 1.5I_{\mathrm{th}}$, the amplitude of the dominant vortex in each laser is approximately five times larger than that of the counter-rotating vortex. This ratio is enhanced as the injection current is increased, reaching 10 for $I = 2.5I_{\mathrm{th}}$. The increase in the relative intensity of one of the vortices indicates the transition from "conventional" lasing to emission of engaged optical vortices.

The steady-state light gears at higher injection currents (from $2I_{\mathrm{th}}$ and higher) are the identical charge antiphase and opposite charge in-phase configurations. The field of these patterns does not reach a zero value in the interlaser spacing, which is in agreement with the selection guidelines to be detailed below. In these configurations, the amplitude of the dominant vortex in each element is approximately ten to 15 times larger than that of the counter-rotating one.

TABLE I. (Color online) Theoretical field patterns for an emitter pair.

Configuration	(a)	(b)	(c)	(d)	(e)
Near-field			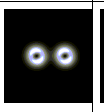		
Phase contour	uniform	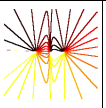	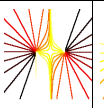	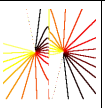	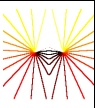
Far-field		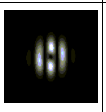	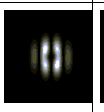		
Vortex configuration	Same amplitude for +/−1 vortices	Same charge In-phase	Same charge Anti-phase	Opposite charge Anti-phase	Opposite charge In-phase
Amplitude ratio		4–8	7–15	5–10	12–16
Injection currents [I_{th}]	1–1.2	1.5–2.5	1.8–4	1.5–2.5	2.3–4

TABLE II. (Color online) Theoretical field patterns for a cyclic five-element emitter, all elements having identical vortex charge.

Configuration	(a)	(b)	(c)	(d)
Near-field	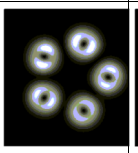	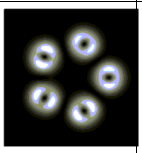	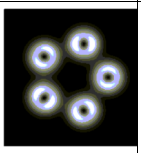	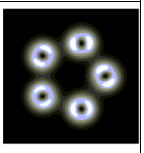
Phase contour	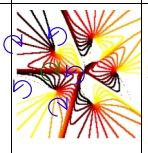	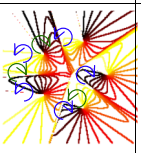	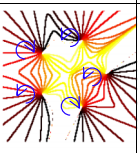	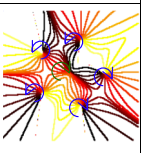
Far-field	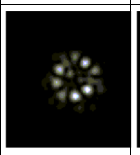	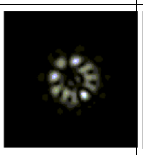	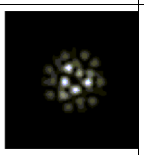	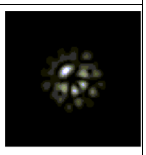
Injection currents [I_{th}]	1.5–2.5	1.5–3	5.1–6	5.1–6

B. Cyclic array of five emitters

The steady-state patterns for the five-element cyclic array are shown in Tables II and III. Table II depicts the patterns in which all the elements emit identical charges: In column (a) is the double-lobe emission pattern, evolving at low injection currents, and in column (b) the in-phase configuration, in which all five vortices have the same topological charge and relative phase, which is the experimentally observed engaged light gear. This configuration evolves at medium injection current levels, and the field of this pattern in the interelement spacing reaches zero amplitude.

The pattern of Table II(c) consists of five identical charge vortices locked with a 144° relative phase difference. In this configuration an additional opposite charge vortex is formed in the center of the array. The phase profile in this configuration is smooth, and the field does not reach zero amplitude in the spacing, thus necessitating relatively high injection currents to evolve.

Note that for an even cyclic array, a smooth phase profile is obtained for the identical charge vortices locked in antiphase while in odd cyclic arrays this configuration is not possible. To obtain a smooth phase profile with nonzero field in the spacing between emitters, the vortices must lock with a phase shift ($2\frac{360}{5} = 144^\circ$ in the five-elements case).

Table III shows four steady-state patterns consisting of nonidentical vortex charges that were found theoretically for a five element array. In configuration (a) the two upper right vortices have the same charge and are in phase, forming another opposite charge vortex between them. The other pairs of neighboring lasers have opposite charge vortices with opposite phases. The field between the emitters reaches zero amplitude, and this configuration evolves at relatively low injection currents.

TABLE III. (Color online) Theoretical field patterns for a cyclic five-element emitter, elements having various vortex charges.

Configuration	(a)	(b)	(c)
Near-field	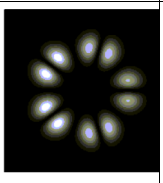	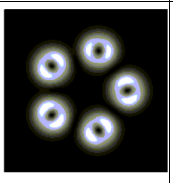	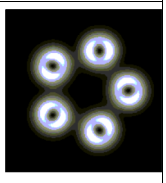
Phase contour		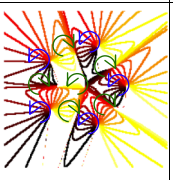	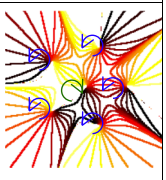
Far-field	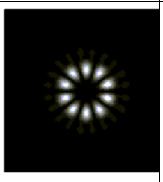	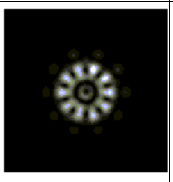	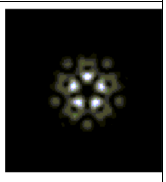
Injection currents [I_{th}]	1–1.3	1.5–3.6	3.6–6

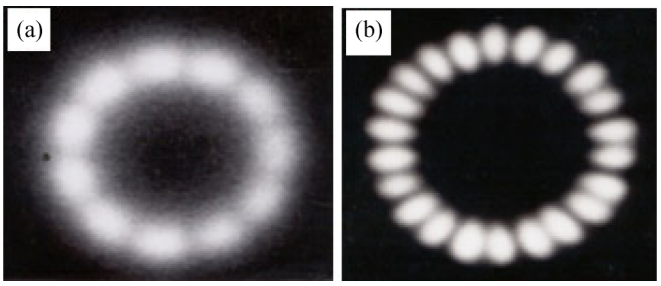

FIG. 8. (Color online) Experimental measurement of emission from 11-elements emitter array (each 10 μm in diameter): (a) spontaneous emission (below threshold) exhibiting the 11 emitting elements, $I_p = 30$ mA, $\tau_{\text{pulse}} = 300$ ns; (b) coherent emission (just above threshold) showing the 11 double-lobed pattern, $I_p = 100$ mA ($I_{\text{th}} = 40$ mA), $\tau_{\text{pulse}} = 300$ ns.

In configuration (b) the three upper left vortices possess identical charge and are in phase, forming additional opposite charge vortices between them. The two remaining vortices on the lower right also have identical charges (opposite to the upper left three), and are locked in phase, again forming an additional opposite charge vortex between them. The field between the lasers reaches zero amplitude, and this configuration appears for low injection currents.

Configuration (c) exhibits identical vortex charges as in configuration (a), but with the opposite phase relation (the identical charge pair is locked with opposite phases, and the opposite charge vortices are locked in phase). This configuration forms a smooth phase profile, and this supermode appears for high injection currents.

Configuration (d) consists of the same vortex charges as configuration (b), but with the opposite phase relation (the identical charge vortices are locked with opposite phases, and the opposite charge vortices are locked in phase). This again forms a smooth phase profile, which is preferred at high injection currents.

C. Pattern selection guidelines

The results of the model detailed above can be compiled to a simple set of guidelines which explain the lasing pattern selection and the engagement rules of the vortices. At low injection currents (close to threshold), both vortices in each emitter element have identical amplitudes (no symmetry breaking), resulting in a standing-wave double-lobe emission (TEM_{10}-like) from each element [column (a) in Tables I and II]. The orientation of the pattern in each laser (the angle of the two lobes) is determined by gain-loss considerations setting the field in the interelement spacing to zero amplitude. For a cyclic array of M emitter array, these configurations form a cyclic array of $2M$ antiphase lobes. These modes are observed also experimentally (see, for example, Fig. 8), but since they do not carry orbital angular momentum, they are not dwelled upon further.

As the injection current is slightly increased, we enter into the regime of the light gears that is the subject of this paper: The gain in the active region is increased and the overlap of the vortex mode with the gain profile becomes more significant. The double-lobed emission from each element, which has a smaller overlap with the gain profile, switches to a predominantly single vortex, which utilizes a larger portion of the gain. The enhanced field-gain overlap of the vortex compensates for the emitter losses in the interelement spacing (the vortex configurations possess more power in the interlaser spacing than the double-lobed emission pattern).

The steady-state relative phase between the vortices in adjacent elements at these medium injection current levels is spontaneously selected to minimize the field in the interemitter spacing (minimizing the modal losses). For a pair of vortices with the same charge, the minimal field between the emitters is achieved for the in-phase configuration. In this configuration the field in the spacing has a zero at a point, not on a line as in the double-lobed emission. For a pair of vortices with opposite charges the configuration which exhibits a null field between elements is the antiphase configuration. Thus all patterns predicted by the model for medium injection levels are characterized by adjacent elements emitting either identical charge vortices which are locked in phase or opposite charge vortices which are locked out of phase.

Increasing further the injection current significantly expands spatial hole burning effects in the gain profile. As a result the gain where the field intensity is relatively low becomes larger, which favors emission with enhanced field in the interelement spacing. These configurations usually exhibit a relatively smooth phase profile (discontinuities in the phase are associated with zero amplitude), which breaks the scheme of two level relative phase charge. Such configurations include out-of-phase locking of identical charge vortices or in-phase locking of opposite charge vortices. Arrays with an odd number of elements may exhibit another locking of identical charge vortices with a phase shift of $2\pi \text{k}/M$ where k is an integer and M is the odd number of elements in the circular array.

Another phenomenon common to all arrays is the transition of the emitted fields from mixed-vortices combination (each laser emits a combination of both the charge $+1$ and the charge -1 vortices) to pure single-headedness vortices as the injection current is increased. At low injection each laser emits both vortices with similar amplitudes, resulting in the TEM_{10}-like modes [see, e.g., column (a) in Tables I and II]. At higher injection levels, a spontaneous symmetry breaking occurs and the emission switches to a vortex mode, but yet each laser still emits the secondary, opposite charge vortex but with smaller amplitude. As the injection current is further increased, the amplitude ratio between the primary and the weak vortices increases, and the emission of each laser in the array consists predominantly of a single vortex.

V. STABILITY ANALYSIS

As mentioned, a striking difference between the theoretical steady state and the experimental results is the richer and diverse variety of theoretically predicted "steady-state" vortices configurations that are not observed experimentally. While the absence of some pattern can be explained by simple gain-loss considerations at a given injection current, the absence of the other patterns requires the understanding of the dynamical stability of the array emission.

The multiple numerical steady-state vortex configurations were found by seeding the structure with multiple random initial conditions at a given current and allowing them to evolve numerically by Eq. (11) to a final, steady-state, configuration. Equation (11) is not the complete physical model, but rather an asymptotic approximation as explained above and thus cannot represent correctly the crucial spatiotemporal carrier dynamics occurring at the experiment when applying the current pulse. As a result, it is possible to theoretically find several locked vortex configurations at a single injection level. The actual dynamical spatiotemporal interplay between the evolution of the field and the gain profile sets a specific evolution trajectory for the field coefficients, which is instrumental in the determination of the stable steady-state pattern and it is not reflected in the steady-state solution of Eq. (11).

To account properly for the complete buildup process of the field and the gain profiles, we simulated the turn-on process of the emitters by starting from a steady-state solution at low injection current and then adiabatically increased the pump level while monitoring the evolving patterns by the temporal solution of the rate equations (11). This is the only way we can apply correctly (physically) this set of equations—performing a series of very small current changes—for each, the carrier dynamics can follow "immediately" and at each step monitor the field pattern. At some current level, the original emission pattern destabilizes, assisted by the numerical noise, and another light gear combination emerges. Although this process is not identical to the experimental procedure we employed, it is the proper way of getting the stable steady-state patterns that we observe.

The results for a five-element cyclic array are discussed here and summarized in Fig. 9 which shows the evolution of the amplitudes of the vortex coefficients as the current level is increased adiabatically. The solid lines mark the amplitudes of the charge $+1$ vortices in each laser, and the dashed lines mark the amplitudes of the charge -1 vortices. Vortices in different lasers are represented by different colors. The in-phase vortex configuration [marked as (a)], which is the one that was observed experimentally, is stable from low to relatively high injection currents. When the injection current is substantially increased, this configuration destabilizes and switches to a pattern in which neighboring lasers are locked with a 144° phase shift between them—marked as (b). Note that the in-phase vortex configuration loses stability only at high pump levels ($\sim 6 I_{\mathrm{th}}$) which were practically unattainable in our experiments without damaging the array. As a result, only the in-phase vortex configuration was observed experimentally.

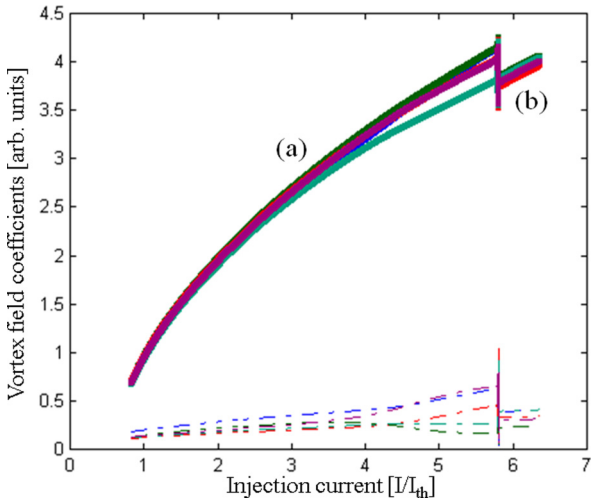

FIG. 9. (Color online) Amplitudes of vortices for a five-laser array, as a function of the injection current. Solid lines $+1$ vortices; dashed lines -1 vortices.

VI. SUMMARY AND CONCLUSIONS

Complex and rich combinations of coupled vortices beams were found to emerge from medium-size linear and circular VCSELs arrays. A theoretical model provided the necessary framework for the understanding of the evolving vortex patterns and their stability properties, exhibiting sound agreement with the experimental results.

For a dimer of coupled VCSELs, two stable configurations were found—each stemmed from different initial conditions (see Table I). These configurations matched perfectly the experimentally observed patterns (antiphase with identical OAM charges and in phase with opposite OAM charges).

For a cyclic array comprising four lasers, two stable configurations were found as well. The antiphase configuration with identical OAM charges was observed experimentally, while the second (two neighboring lasers in phase and with opposite OAM charges and an antiphase pair with identical charges) was not. For cyclic arrays of an odd number of VCSELs we found several theoretically possible configurations (Tables II and III). The in-phase structure with identically charged vortices was observed experimentally while the others were not. Stability analysis (Fig. 9) shows that the in-phase configuration in odd cyclic arrays is stable for low injection levels and is therefore more likely to be observed experimentally. The other possible configurations evolve at relatively high current injection levels (approximately three to four times the threshold current), which was difficult to achieve experimentally because of excessive heating of the sample.

It should be mentioned that the same theoretical analysis predicts also regions of multistable gear patterns and hysteresis [52]. Such dynamical behavior is fundamentally interesting as well as practically important because it may enable storage and processing of the "bits" embedded in the optical pattern.

The vortex charges and the related angular momentum enable the formation of complex beam configurations which carry OAM and were not observed previously in laser arrays. While arrays of optical vortices can be engineered *linearly* by means of interference using spatial light modulators (SLMs) and computer generated holograms, such systems are bulky and, especially in the case of SLMs, quite expensive. VCSEL arrays on the other hand form a compact, fully integrated and low-cost source for complex vortex patterns and beams which can be controlled and modified to some level by the injection current properties [54]. Such beams allow for multiple bits encoding on a single photon or pulse, and can be employed for fast classical and quantum communications, particle trapping, and subdiffraction limit imaging.

[1] A. Mair, A. Vaziri, G. Weihs, and A. Zeilinger, Nature **412**, 313 (2001).

[2] A. Vaziri, G. Weihs, and A. Zeilinger, J. Opt. B **4**, S47 (2002).

[3] G. Molina-Terriza, A. Vaziri, J. Řeháček, Z. Hradil, and A. Zeilinger, Phys. Rev. Lett. **92**, 167903 (2004).

[4] J. P. Torres, Y. Deyanova, L. Torner, and G. Molina-Terriza, Phys. Rev. A **67**, 052313 (2003).

[5] A. Vaziri, G. Weihs, and A. Zeilinger, Phys. Rev. Lett. **89**, 240401 (2002).

[6] N. K. Langford, R. B. Dalton, M. D. Harvey, J. L. O'Brien, G. J. Pryde, A. Gilchrist, S. D. Bartlett, and A. G. White, Phys. Rev. Lett. **93**, 053601 (2004).

[7] G. Molina-Terriza, A. Vaziri, R. Ursin, and A. Zeilinger, Phys. Rev. Lett. **94**, 040501 (2005).

[8] J. Wang, J-Y. Yang, I. M. Fazal, N. Ahmed, Y. Yan, H. Huang, Y. Ren, Y. Yue, S. Dolinar, M. Tur, and A. E. Willner, Nat. Photonics **6**, 488 (2012).

[9] N. Bozinovic, Y. Yue, Y. Ren, M. Tur, P. Kristensen, H. Huang, A. E. Willner, and S. Ramachandran, Science **340**, 1545 (2013).

[10] S. W. Hell, Science. **316**, 1153 (2007).

[11] K. I. Willig, S. O. Rizzoli, V. Westphal, R. Jahn, and S. W. Hell, Nature **440**, 935 (2006).

[12] H. He, M. E. J. Friese, N. R. Heckenberg, and H. Rubinsztein-Dunlop, Phys. Rev. Lett. **75**, 826 (1995).

[13] K. Dholakia, G. Spalding, and M. MacDonald, Phys. World **15**, 31 (2002).

[14] D. G. Grier, Nature **424**, 810 (2003).

[15] J. Scheuer and M. Orenstein, J. Opt. Soc. Am. B. **22**, 1260 (2005).

[16] P. Galajda and P. Ormos, Appl. Phys. Lett. **78**, 249 (2001).

[17] K. Ladavac and D. G. Grier, Opt. Express **12**, 1144 (2004).

[18] G. Gibson, J. Courtial, M. J. Padgett, M. Vasnetsov, V. Pas'ko, S. M. Barnett, and S. Franke-Arnold, Opt. Express **12**, 5448 (2004).

[19] J. H. Lee, G. Foo, E. G. Johnson, and G. A. Swartzlander, Phys. Rev. Lett. **97**, 053901 (2006).

[20] A. Jesacher, A. Schwaighofer, S. Furhapter, C. Maurer, S. Bernet, and M. Ritsch-Marte, Opt. Exp. **15**, 5801 (2007).

[21] G. Swartzlander, Opt. Photonics News **17**, 39 (2006).

[22] P. Genevet, S. Barland, M. Giudici, and J. R. Tredicce, Phys Rev. Lett. **104**, 223902 (2010).

[23] J. Masajada, I. Augustyniak, and A. Popiołek-Masajada, J. Opt. **15**, 044031 (2013).

[24] L. Allen, M. J. Padgett, and M. Babiker, Prog. Opt. **39**, 291 (1999).

[25] M. S. Soskin and M. V. Vasnetsov, Prog. Opt. **42**, 219 (2001).

[26] G. Indebetouw, J. Mod. Opt. **40**, 73 (1993).

[27] G. Molina-Terriza, J. P. Torres, And L. Torrner, Nat. Phys. **3**, 305 (2007).

[28] A. M. Yao and M. J. Padgett, Adv. Opt. Photon. **3**, 161 (2011).

[29] P. Coullet1, L. Gil, and F. Rocca, Opt. Commun. **73**, 403 (1989).

[30] A. S. Desyatnikov, Y. S. Kivshar, and L. Torner, Prog. Opt. **47**, 291 (2005).

[31] G. A. Swartzlander, Jr. and C. T. Law, Phys. Rev. Lett. **69**, 2503 (1992).

[32] A. S. Desyatnikov, A. A. Sukhorukov, and Y. S. Kivshar, Phys. Rev. Lett. **95**, 203904 (2005).

[33] S. Lopez-Aguayo, A. S. Desyatnikov, and Y. S. Kivshar, Opt. Express **14**, 7903 (2006).

[34] A. S. Desyatnikov and Yu. S. Kivshar, Phys. Rev. Lett. **88**, 053901 (2002).

[35] T. Carmon, R. Uzdin, C. Pigier, Z. H. Musslimani, M. Segev, and A. Nepomnyashchy, Phys. Rev. Lett. **87**, 143901 (2001).

[36] S. Lopez-Aguayo, A. S. Desyatnikov, Y. S. Kivshar, S. Skupin, W. Krolikowski, and O. Bang, Opt. Lett. **31**, 1100 (2006).

[37] J. R. Hayes, E. G. Paek, A. Scherer, and Y. S. Kwon, IEEE J. Quantum Electron. **26**, 1039 (1990).

[38] G. Molina-Terriza, J. Recolons, and L. Torner, Opt. Lett. **25**, 1135 (2000).

[39] H. Pier, E. Kapon, and M. Moser, Nature **407**, 880 (2000).

[40] M. Orenstein, E. Kapon, N. G. Stoffel, J. P. Harbison, L. T. Florez, and J. Wullert, Appl. Phys. Lett. **58**, 804 (1991).

[41] M. E. Warren, P. L. Gourley, G. R. Hadley, G. A. Vawter, T. M. Brennan, B. E. Hammons, and K. L. Lear Sandia, Appl. Phys. Lett. **61**, 1484 (1992).

[42] D. K. Serkland, K. D. Choquette, G. R. Hadley, K. M. Geib, and A. A. Allerman, Appl. Phys. Lett. **75**, 3754 (1999).

[43] L. D. A. Lundeberg, D. L. Boiko, and E. Kapon, J. Sel. Top. Quantum Electron. **13**, 1309 (2007).

[44] D. Zhou and L. J. Mawsta, Appl. Phys. Lett. **77**, 2307 (2000).

[45] J. J. Raftery, Jr., A. C. Lehman, A. J. Danner, P. O. Leisher, A. V. Giannopoulos, and K. D. Choquette, Appl. Phys. Lett. **89**, 081119 (2006).

[46] D. F. Siriani and K. D. Choquette, Electron. Lett. **46**, 712 (2010).

[47] M. Brambila, F. Battipede, L. A. Lugiato, V. Penna, F. Prati, C. Tamm, and C. O. Weiss, Phys. Rev. A **43**, 5090 (1991).

[48] K. Otsuka and S-C. Chu, Opt. Lett. **34**, 10 (2009).

[49] J. Scheuer and M. Orenstein, Science **285**, 230 (1999).

[50] The vortex charge was determined from the LP interference pattern (Fig. 4). We interfered a magnified image of the LP pattern with a reference plane wave, which was derived by spatial filtering a portion of the emission of one of the array elements. Due to the phase discontinuity when crossing the vortex, constructive interference on one side of the vortex becomes destructive on the other side, and one interference fringe disappears. The direction of the disappearance depends on the sign of the topological charge. Figure 4(a) depicts the vanishing of an interference fringe in each of the two coupled vortices, having opposite charges (left vortex: the fringe disappears from top to bottom; right vortex: it disappears from bottom to top). Figure 4(b) is the recorded interference pattern for a pair of vortices with the same topological charges.

[51] T. Fishman and M. Orenstein, Opt. Lett. **21**, 600 (1996).

[52] Y. Yadin, J. Scheuer, Y. Gross, and M. Orenstein, in *Proceedings of Lasers and Electro-Optics Society 2000 Annual Meeting* (IEEE, San Juan, Puerto Rico, 2000), Vol. 1, pp. 133–134.

[53] G. P. Agrawal and N. K. Dutta, *Long-Wavelength Semiconductor Lasers* (Van Nostrand Reinhold, New York, 1986).

[54] For example, if one needs a predefined complex angular momenta decorated beam for some application, a 100-μm-size VCSEL array chip (for ~$1 US) will be much more efficient and inexpensive compared to any other alternative.